Abstract #04197 ISMRM ABSTRACT

Magnetic resonance fingerprinting reconstruction using spatiotemporal maps and implicit neural representation

Primary: Acquisition & Reconstruction - Quantitative Imaging: relaxometry, multi-parametric, MR Fingerprinting, and synthetic MRI) **Secondary:** Acquisition & Reconstruction - Image Reconstruction: AI) **Presentation:** PowerPitch Oral, Oral, Digital Poster, Traditional Poster) **Keywords:** MR FINGERPRINTING SIGNAL REPRESENTATIONS AI/ML IMAGE RECONSTRUCTION DYNAMIC MRI RECONSTRUCTION LOW RANK

Rodrigo Lobos[1], **Christopher E Keen**[2], **Sydney Kaplan**[1,2,3], **Hongze Yu**[1,4], **Yun Jiang**[1,2,3], **Nicole Seiberlich**[1,2,3], **Jon-Fredrik Nielsen**[1,2,3,4,5], **Jeffrey A Fessler**[2,3,4,6,7], **Douglas Noll**[1]

[1]University of Michigan, Ann Arbor, MI, United States of America
[2]Department of Biomedical Engineering, University of Michigan, Ann Arbor, MI, United States of America
[3]Department of Radiology, University of Michigan, Ann Arbor, MI, United States of America
[4]Electrical Engineering and Computer Science, University of Michigan, Ann Arbor, MI, United States of America
[5]Functional MRI Laboratory, Department of Radiology, University of Michigan, Ann Arbor, MI, United States of America
[6]ECE, University of Michigan, Ann Arbor, MI, United States of America
[7]Department of Electrical and Computer Engineering, University of Michigan, Ann Arbor, MI, United States of America

Presenting Author: *Rodrigo Lobos (rlobos@umich.edu)*

Impact

The proposed reconstruction framework utilizes a signal model with enhanced representation capabilities that reduces the number of unknowns (i.e., coefficient images) compared to using a low-rank model learned from a dictionary, facilitating reconstruction.

Synopsis

Motivation: **Standard methods for magnetic resonance fingerprinting (MRF) reconstruction commonly adopt a low-rank model to approximate the MRF dynamic signal. However, many coefficient images might be needed for an accurate representation, and biases can be introduced if insufficient coefficient images are considered.**

Goals: **To propose a novel MRF reconstruction framework that uses a parsimonious model based on spatiotemporal maps (STM).**

Approach: **STM parameters are calculated from autocalibration data using variable density spirals.**

Results: **The STM model provides a more parsimonious representation than the low-rank model, and can be combined with modern regularizers (e.g., implicit neural representation) for MRF reconstruction.**

Introduction

Many MRF reconstruction methods rely on a low-rank model learned from synthetic data[1-6]. Specifically, the dynamic signal at each voxel is represented as a linear combination of the same set of temporal basis functions learned from a dictionary, where the scalar coefficient maps are estimated by solving an inverse problem. However, in cases where the temporal characteristics vary considerably across spatial locations, the number of temporal functions to accurately represent dynamic changes for all voxels tends to increase[7]. This increases the number of coefficients that need to be recovered, which limits the acceleration factor as more unknowns should be estimated from undersampled data. In this work, we improve the representation by adopting a model based on spatiotemporal maps[8] (STM). In the STM model, a different set of temporal functions (a.k.a spatiotemporal maps) is learned for each voxel from autocalibration data, by leveraging the autoregressive properties of (k, t)-space. STMs can provide a more parsimonious representation than low-rank models, decreasing the number of temporal functions needed for each voxel. We show that STMs can be synergistically combined with modern regularizers (e.g., implicit neural representation) for enhanced MRF reconstruction.

Theory

Let $\rho(\vec{x},n)$ denote the dynamic MRF signal at one voxel where $n\in\{1,\dots,N\}$ indexes each time frame in the acquisition. The STM model has the form $\rho(\vec{x},n)\approx\sum_{l=1}^{L}s_l(\vec{x},n)\rho_l(\vec{x})$ where $\{\rho_l(\vec{x})\}$ are the coefficient images and $\{s_l(\vec{x},n)\}$ are the voxel-dependent spatiotemporal maps. STMs are calculated from autocalibration data acquired in each time frame.

We reconstruct coefficient images by minimizing the cost function

$$F(\boldsymbol{\rho}_1,\dots,\boldsymbol{\rho}_L)=\|\mathcal{A}(\sum_{l=1}^{L}\boldsymbol{S}_l\boldsymbol{\rho}_l)-\boldsymbol{y}\|_2^2+R(\boldsymbol{\rho}_1,\dots,\boldsymbol{\rho}_L)$$

where $\boldsymbol{S}_l$ and $\boldsymbol{\rho}_l$ are the STMs in matrix form and vectorized coefficient images, respectively, including all voxels and time frames; $\mathcal{A}$ is a forward operator including the nonuniform Fourier transform, coil sensitivities, and a self-weighting operation; $\boldsymbol{y}$ is the non-Cartesian data acquired in each time frame; and R is a regularizer. We minimize F using a TV regularizer by representing $\{\boldsymbol{\rho}_l\}$ with an implicit neural representation[9] (INR) where each coefficient image corresponds to a different output of a single INR.

Methods

We first assessed the representation capabilities of the STM model on a simulated single-channel MRF dataset using an XCAT phantom, and compared it with the low-rank model representation using 5 and 11 temporal functions. Secondly, we assessed the reconstruction framework using retrospectively undersampled simulated data, and prospectively undersampled multichannel data obtained from a NIST phantom and an *in vivo* brain acquisition. We implemented the STM+INR reconstruction using the guidelines by Yu et al.[9], and compared with the low-rank method using 5 temporal functions. We used FISP-based MRF sequences[10, 11] with varying flip angle and constant TR to acquire each dataset. We used a golden angle variable density spiral acquisition where a densely sampled center k-space region was included in each time frame as autocalibration data for STM computation. STMs were computed using PISCO[8, 12] after gridding the autocalibration data and $L = 3$ components were considered. T1, T2, and proton density maps were calculated using a pattern-matching approach with a predesigned dictionary.

Results

Figure 1.a shows the time course for one voxel of the simulated data and the approximations using the STM model and the low-rank model. The STM model using only 3 temporal functions for each voxel accurately approximated the ground-truth values, obtaining similar results to the low-rank model using 11 temporal functions. There was a mismatch when using the low-rank model with 5 temporal functions. Figure 1.c shows the time courses of different reconstructions. The proposed reconstruction framework using STM+INR obtained the best result. Figure 2 shows the parameter maps after reconstruction, with STM+INR obtaining the best quantitative results.

Figure 3 shows the parameter maps for each reconstruction using the NIST phantom data. Both methods provided good estimations of T1 as shown in Fig.4; however, high T2 values were overestimated when using STM+INR and underestimated when using the low-rank method. Better agreement was obtained for low T2 values when using STM+INR. Similar qualitative results were observed in the brain dataset, as shown in Fig. 5. Compared to low-rank reconstruction, STM+INR exhibited fewer aliasing artifacts.

Discussion and Conclusions

The STM model can provide a more parsimonious representation for the MRF dynamic signal than the low-rank model, which can be leveraged in the reconstruction of accelerated data using modern regularizers.

Acknowledgements

This work was supported by NIH grants R21EB034344, R01EB035618, R37CA263583, and R01CA284172.

References

1. [1] McGivney, D.F., Pierre, E., Ma, D., Jiang, Y., Saybasili, H., Gulani, V. and Griswold, M.A., 2014. SVD compression for magnetic resonance fingerprinting in the time domain. IEEE transactions on medical imaging, 33(12), pp.2311-2322.
https://doi.org/10.1109/TMI.2014.2337321

2. [2] Zhao, B., Setsompop, K., Adalsteinsson, E., Gagoski, B., Ye, H., Ma, D., Jiang, Y., Ellen Grant, P., Griswold, M.A. and Wald, L.L., 2018. Improved magnetic resonance fingerprinting reconstruction with low-rank and subspace modeling. Magnetic resonance in medicine, 79(2), pp.933-942.
https://doi.org/10.1002/mrm.26701

3. [3] Assländer, J., Cloos, M.A., Knoll, F., Sodickson, D.K., Hennig, J. and Lattanzi, R., 2018. Low rank alternating direction method of multipliers reconstruction for MR fingerprinting. Magnetic resonance in medicine, 79(1), pp.83-96.
https://doi.org/10.1002/mrm.26639

4. [4] Doneva, M., Amthor, T., Koken, P., Sommer, K. and Börnert, P., 2017. Matrix completion-based reconstruction for undersampled magnetic resonance fingerprinting data. Magnetic resonance imaging, 41, pp.41-52.
https://doi.org/10.1016/j.mri.2017.02.007

5. [5] Hamilton, J.I., Truesdell, W., Galizia, M., Burris, N., Agarwal, P. and Seiberlich, N., 2023. A low-rank deep image prior reconstruction for free-breathing ungated spiral functional CMR at 0.55 T and 1.5 T. Magnetic Resonance Materials in Physics, Biology and Medicine, 36(3), pp.451-464.
https://doi.org/10.1007/s10334-023-01088-w

6. [6] Cruz, G., Qi, H., Jaubert, O., Kuestner, T., Schneider, T., Botnar, R.M. and Prieto, C., 2022. Generalized low-rank nonrigid motion-corrected reconstruction for MR fingerprinting. Magnetic Resonance in Medicine, 87(2), pp.746-763.
https://doi.org/10.1002/mrm.29027

7. [7] Liang, Z.P., 2007, April. Spatiotemporal imaging with partially separable functions. In 2007 4th IEEE international symposium on biomedical imaging: from nano to macro (pp. 988-991). IEEE.
https://doi.org/10.1109/NFSI-ICFBI.2007.4387720

8. [8] Lobos, R.A., Wang, X., Fung, R.T., He, Y., Frey, D., Gupta, D., Liu, Z., Fessler, J.A. and Noll, D.C., 2025. Spatiotemporal Maps for Dynamic MRI Reconstruction. arXiv preprint arXiv:2507.14429.
https://doi.org/10.48550/arXiv.2507.14429

9. [9] Yu, H., Fessler, J.A. and Jiang, Y., 2025. Bilevel optimized implicit neural representation for scan-specific accelerated mri reconstruction. arXiv preprint arXiv:2502.21292.
https://doi.org/10.48550/arXiv.2502.21292

10. [10] Hamilton, J.I., Jiang, Y., Chen, Y., Ma, D., Lo, W.C., Griswold, M. and Seiberlich, N., 2017. MR fingerprinting for rapid quantification of myocardial T1, T2, and proton spin density. Magnetic resonance in medicine, 77(4), pp.1446-1458.
https://doi.org/10.1002/mrm.26216

11. [11] Jiang, Y., Ma, D., Seiberlich, N., Gulani, V. and Griswold, M.A., 2015. MR fingerprinting using fast imaging with steady state precession (FISP) with spiral readout. Magnetic resonance in medicine, 74(6), pp.1621-1631.
https://doi.org/10.1002/mrm.25559

12. [12] Lobos, R.A., Chan, C.C. and Haldar, J.P., 2023. New theory and faster computations for subspace-based sensitivity map estimation in multichannel MRI. IEEE

transactions on medical imaging, 43(1), pp.286-296.
https://doi.org/10.1109/TMI.2023.3297851

Figures and Tables

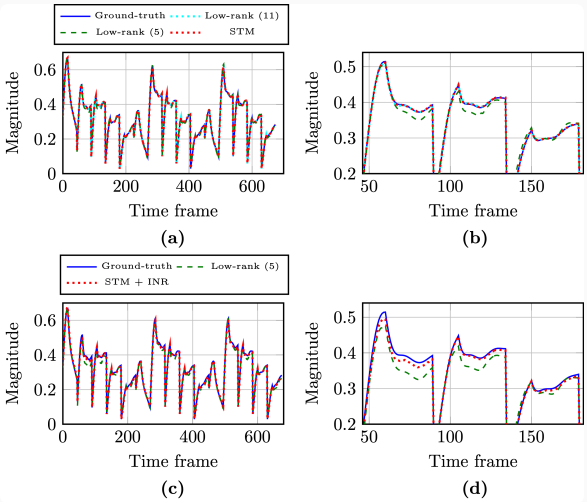

Scan for high-resolution version

Figure 1: Signal evolution for one voxel to examine representation and reconstruction capabilities. Representation: (a) Ground-truth and the approximations given by the STM model using L =3 and the low-rank model using 5 and 11 temporal functions. The coefficient images in each case are directly calculated from the fully sampled data to assess representation. (b) Zoomed-in version of (a). Reconstruction:(c) Ground-truth and the reconstructions from undersampled data. (d) Zoomed-in version of (c).

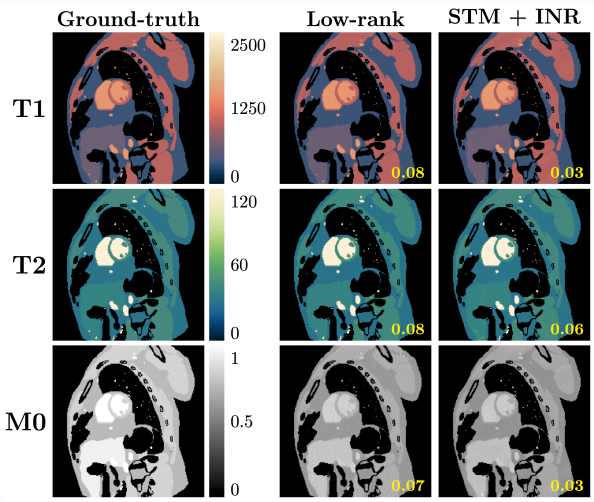

Scan for high-resolution version

Figure 2: Parameter maps obtained after reconstructing the retrospectively undersampled simulated data using the XCAT phantom. The normalized-root-mean-square error (NRMSE) with respect to the ground-truth is shown in each case in the bottom right corner. The STM+INR reconstructions have lower NRMSE while using fewer coefficient images.

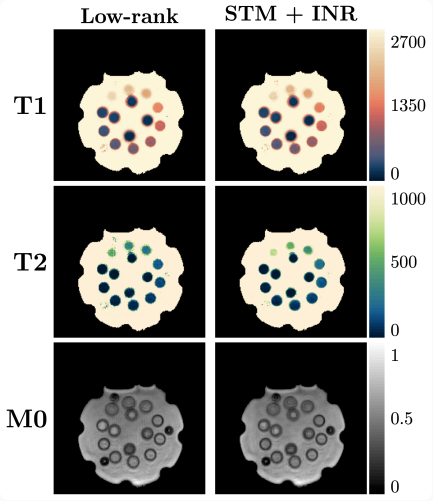

Scan for high-resolution version

Figure 3: Parameter maps obtained after reconstructing the prospectively undersampled data using the NIST phantom.

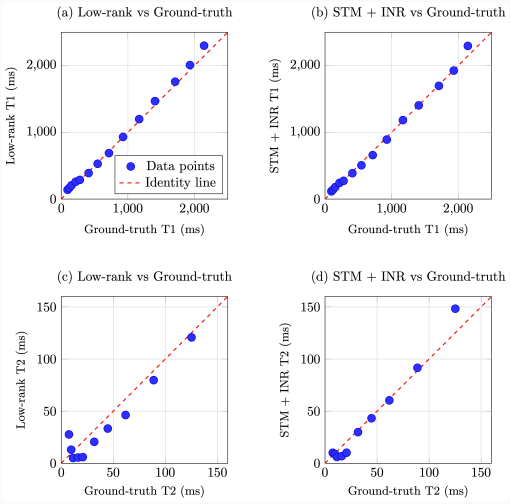

Scan for high-resolution version

Figure 4: Comparison of the T1 and T2 values obtained by the two reconstruction methods with the nominal values of the NIST phantom in 14 and 10 regions of interest, respectively. The mean was calculated within each ROI.

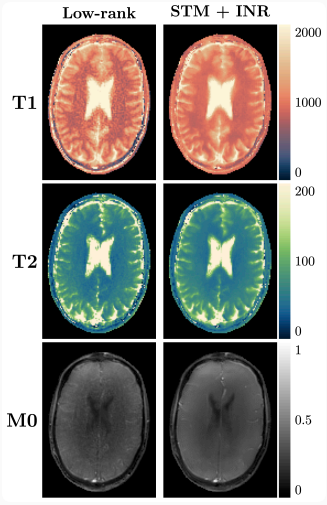

Scan for high-resolution version

Figure 5: Parameter maps obtained after reconstructing the prospectively undersampled in vivo brain data. Less aliasing artifacts are observed in the parameter maps derived from the STM+INR reconstruction.